Specific heat of bcc ^{3}He

D. S. Greywall
Bell Laboratories, Murray Hill, New Jersey 07974
(Received 19 November 1976)

The specific heat of bcc ^{3}He has been measured at five molar volumes between 21.5 and 24.5 cm^3 and for temperatures between 50 mK and the melting curve. The data below 0.5 K show no evidence of the large anomalous contribution to the specific heat which has been observed in all previous measurements, indicating that this anomaly is not due to an intrinsic property of this quantum solid. Values of the nuclear exchange energy derived from the low-temperature data are in good agreement with values determined by others from various types of measurements. The specific-heat data above approximately 0.5 K are in agreement with previous results and show the large contribution which is generally attributed to thermally activated vacancies. Because of the absence in the present work of the low-temperature anomaly, however, the temperature dependence of the vacancy contribution could be determined more accurately than was previously possible. The measured vacancy contribution shows significant deviations from the expected behavior.

I. INTRODUCTION

In this paper precise measurements of the constant-volume specific heat C_V of bcc ^{3}He are reported. The data were obtained along five different isochores between 21.5 and 24.5 cm^3/mole and at the three largest molar volumes extend in temperature from 50 mK to the melting curve. It had been the intention to concentrate on measurements below roughly 0.5 K and to determine as precisely as possible the temperature dependence of the large anomalous contribution to the specific heat observed in all of the previous C_V measurements[1-4] on bcc ^{3}He in this temperature range. It was anticipated that such measurements would yield meaningful indications as to possible sources[5-12] of this long-standing anomaly. Instead, the data show no evidence of the anomalous contribution at all. The results at low temperatures ($T \lesssim 0.3$ K) can be described well as being due only to the nuclear spins, which provide a contribution to the specific heat proportional to T^{-2}, and to the phonons, which account for the T^3 contribution. The best-fit coefficients of these two terms correspond to values of the exchange energy $|J|$ and the Debye temperature at 0 K, Θ_0, which are in agreement with other experiments. Thus it is demonstrated that the large excess specific heat observed previously is not due to an intrinsic property of this quantum solid.

At higher temperatures, the present results are in general agreement with the earlier measurements[1-4] and indicate a contribution to the specific heat which becomes very appreciable near the melting temperature and which has generally been attributed to the presence of thermally activated vacancies. The present data, however, show significant deviations from the expected temperature dependence for this contribution. Because of the absence in this work of the low-temperature anomaly, the vacancy contribution could be determined more accurately than was previously possible. A brief report on a portion of this work has previously been published.[13]

II. EXPERIMENTAL DETAILS

A. Calorimeter

A cross-sectional drawing of the cylindrical calorimeter is shown in Fig. 1. It was constructed of copper and had a nominal mass of 190 g and a nominal sample-chamber volume of 9 cm^3. The calorimeter was firmly positioned below the mixing chamber of a dilution refrigerator (Fig. 2) using three graphite[14,15] tubes (2.7-mm i.d., 4.8-mm o.d.) which were attached to the sample cell via a cop-

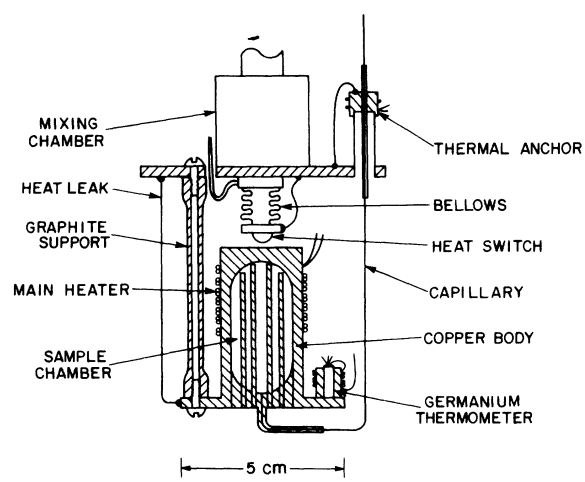

FIG. 1. Calorimeter.

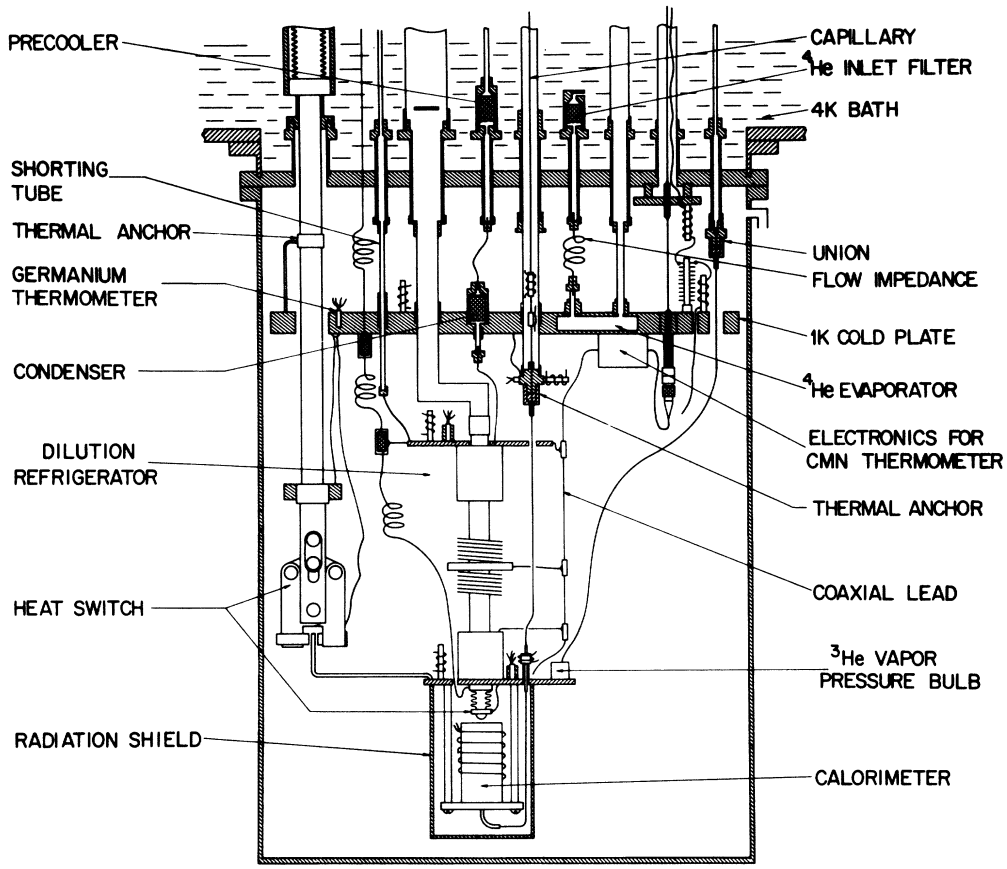

FIG. 2. Cryostat.

per flange machined as part of the cell body. This flange was also the platform on which three germanium resistors and a cerium-magnesium-nitrate (CMN) thermometer (see Sec. II D) were mounted. The calorimeter was completely surrounded by a copper shield at the mixing-chamber temperature.

In order to make precise specific-heat measurements it is important to keep the specific heat of the empty calorimeter as small as possible relative to that of the sample. It is also desirable that the material from which the calorimeter is made have a high thermal conductivity to ensure isothermal conditions. For these reasons oxygen-free high-conductivity copper was chosen as the construction material over, for example, BeCu. Although copper is not a high-strength material, this was not a serious draw back since in this experiment the pressure in the sample chamber was always less than 100 bar.

For temperatures greater than approximately 50 mK the Kapitza thermal-boundary resistance is usually not a serious problem. Since in this work no measurements were made at significantly lower temperatures, it was not necessary to greatly increase the surface area by filling the calorimeter with fine copper wires[4] or sintered copper sponge.[3] Had this modification been made, it may have been responsible for large density gradients in the sample or numerous crystal defects, either of which would have seriously affected the specific-heat measurements. There were however 12 0.15-cm-diam copper rods passing through the sample chamber. Although the presence of these rods did increase the surface area by a factor of 2, their main purpose was to reduce the average distance of the sample from the nearly isothermal surface of the calorimeter and thereby reduce the time necessary for thermal equilibrium to be established. These copper rods and the bottom end plug were soldered[16] to the body of the calorimeter in a hydrogen atmosphere in order to keep the inner surface of the sample chamber clean. The calorimeter was then vacuum annealed at 500 °C for several hours to remove the hydrogen which had diffused into the copper.

The stainless-steel filling capillary which entered the sample chamber through the bottom end

plug of the calorimeter had a 0.05-mm i.d., a 0.15-mm o.d., and was approximately 8 cm long up to the thermal anchor on the mixing-chamber platform. This very small capillary size was chosen mainly to reduce the relative importance of the capillary's contribution to the measured heat capacity.

The main heater (10 kΩ), an auxiliary heater (10 kΩ), and two thermometer-bridge reference resistors (1600 Ω, 2000 Ω) (see Sec. II D) were non-inductively wound around and varnished (GE 7031) to the body of the calorimeter. Heavy-enamel-insulated 0.023-mm-diam platinum-tungsten (92%, 8%) resistance wire[17] was used because of its high and nearly-temperature-independent resistance and its small specific heat at low temperatures.[18,19] The electrical leads connecting these resistors and the germanium thermometers to the terminal strip on the mixing chamber were 0.076-mm-diam niobium wires.

A fine copper wire providing a conduction of approximately 10^{-7} W/K at 0.1 K was connected between the calorimeter and the mixing chamber. The wire was used to counterbalance the residual heat leak of 2 nW into the cell and was used in conjunction with the auxiliary heater to adjust the temperature drift rates.

The time required to solidify the helium sample or to cool the calorimeter to the lowest temperatures was considerably shortened by closing the hydraulically operated (liquid-^{4}He) heat switch. Both contact surfaces of the heat switch were gold plated. The effectiveness of the switch is shown in Fig. 3 where the heat input to the calorimeter divided by the resulting temperature difference between the calorimeter and mixing chamber is plotted as a function of the calorimeter temperature (T_{hot}). The upper curve is the conductance measured with the heat switch closed under a force of 36 N; the lower curve was determined with the heat switch open and corresponds to the combined conductances of the graphite support tubes, the niobium leads, and the copper-wire thermal link. The dashed portion of each curve was determined assuming that the heat input to the calorimeter was due only to the power dissipated in the auxiliary heater. The solid curves were determined assuming that there was an additional heat leak of 2 nW. When the heat switch was opened, approximately 2.6 μJ of heat was generated ($Q/F = 0.07$ μJ/N).

The cryostat was mounted on a vibration-isolation table which was very effective in reducing the heat leak to the calorimeter. Vibration heat leaks[20] are, however, roughly proportional to the mass of the calorimeter and for a good isolation system are of the order of 10 nW/kg. The heat

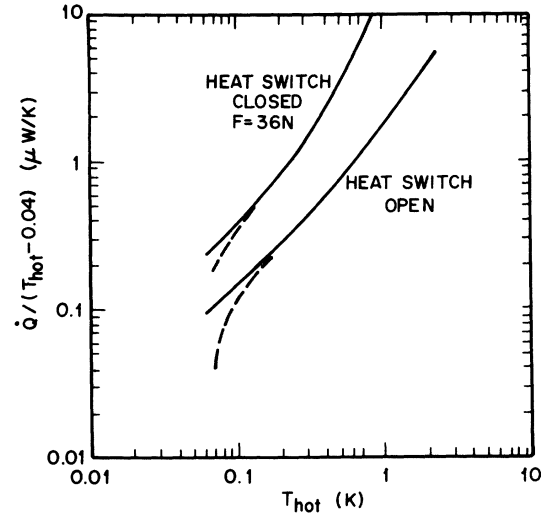

FIG. 3. Measured conductance between the mixing chamber ($T \approx 0.04$ K) and the calorimeter (T_{hot}) with the heat switch closed and with the heat switch open. Other details are given in the text.

leak into the 190-g calorimeter of 2 nW is therefore reasonable.

B. Sample-chamber volume

The room-temperature volume of the sample chamber was determined using the accurately measured change in pressure as ^{4}He gas contained initially only in the sample chamber was expanded into a calibrated 50-cm^3 reference volume. A correction was then applied for the thermal contraction (≈1%) of the copper cell in order to arrive at its low-temperature volume, namely, 8.97 ± 0.02 cm^3. No corrections were made for the change in volume as the cell was brought up to working pressure since this change was calculated to be always less than 0.1%.

C. ^{3}He sample and pressure generator

The ^{3}He gas sample was purified by distillation[21] and had a ^{4}He impurity concentration determined by mass spectrometry[22] of 2.40 ± 0.05 ppm.

The high-purity ^{3}He which was stored near atmospheric pressure was brought up to working pressure using an adsorption pump. The small stainless-steel bulb (25 cm^3) containing the activated charcoal was connected to the ^{3}He storage cylinders via a large-diameter capillary. There was a trap (77 K) in this line containing molecular sieve material. To generate the pressure, the bulb was first lowered into a liquid-^{4}He Dewar and left in this position until pumping had essentially

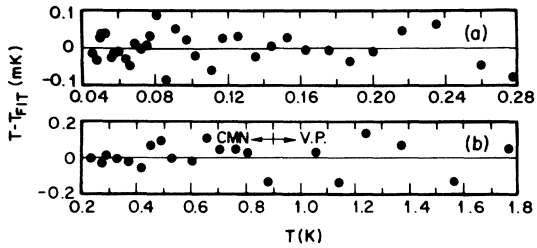

FIG. 4. Deviations of the thermometer calibrations from the least-squares polynominal fits to these data. (a) Bridge 1; (b) bridge 2.

ceased. After manipulating the appropriate valves in the gas handling manifold the bulb was then pulled from the Dewar creating a ^{3}He pressure in the bulb of about 150 bar. A metering valve in the line now joining the high-pressure bulb to the calorimeter was slowly opened to increase the sample pressure. It was necessary to temperature cycle the pump several times in order to generate the desired pressure in the calorimeter.

D. Thermometry

The temperature was measured using two germanium thermometers[23,24] in separate ac resistance bridges.[25] Bridge 1 was used in the temperature range $0.040 < T < 0.26$ K; bridge 2 in the range $0.26 < T < 2.0$ K. For temperatures greater than 0.9 K, bridge 2 was calibrated against a third germanium thermometer (in a dc circuit) which had been previously calibrated using the vapor pressure of ^{3}He (1962 vapor-pressure scale[26]). For $T < 0.9$ K, both bridges were calibrated against the magnetic susceptibility of CMN.

The bridge-ratio–versus–temperature data for each bridge were fitted to the polynomial

$$\ln T = \sum_{i=0}^{N} A_i (\ln R)^i , \tag{1}$$

with the resistance $R = R_{\rm ref}\mathcal{R}/(1-\mathcal{R})$. Here $\mathcal{R}$ is the bridge ratio and $R_{\rm ref}$ is the temperature-independent resistance of the reference resistor. The deviations from the fit for bridge 1 with $N = 6$ are shown in Fig. 4(a) and for bridge 2 with $N = 8$ in Fig. 4(b).

With bridge 1 the temperature could be determined with a precision of at least 0.015% of T making it possible to measure 5% changes in T (for the specific-heat data) to a precision of better than 0.3%. Above 0.26 K, 5% changes in T could be determined using bridge 2 with a precision of better than 0.1%. In order to achieve the stated thermometer resolution at the lowest temperatures, it was necessary to dissipate 5×10^{-12} W of power in the germanium thermometer of bridge 1. Because of the self-heating in the resistor, this power dissipation warmed the thermometer approximately 0.3 mK above the sample temperature at 60 mK. The voltage amplitudes of the oscillator driving the bridge circuit was however sufficiently stable that changes in the level of self heating were less than the resolution of the thermometer. There were thus no problems arising from the fact that the thermometers were not calibrated using their zero-power resistance.

A cross-sectional drawing of the CMN thermometer is shown in Fig. 5. Finely powdered CMN mixed with Apiezon-N grease was packed along with 100 No. 40 bare copper wires into a 150-μH coil. The ends of the fine wires were soldered[16] into a threaded copper stud. Epoxy was used to support and to encapsulate the filled coil. The magnetic susceptibility of the 10-mg CMN sample was determined by measuring the resonant frequency of an LC tank circuit[27-32] driven by a tunnel diode[33] and operating near 850 kHz. A miniature superconducting coaxial cable joined the CMN thermometer, mounted on the calorimeter to the tank capacitor and tunnel diode mounted on the 1-K platform. When averaged over 10 sec, the oscillator frequency was stable over a period of several hours to 1 part in 10^7.

The resonant frequency of the tank circuit is given by

$$f = 1/2\pi(LC)^{1/2} , \tag{2}$$

where

$$L = L_0(1+4\pi\chi) \tag{3}$$

and

$$\chi = \chi_0 + \eta\Lambda/(T-\Delta) . \tag{4}$$

In these expressions L_0 is the inductance of the

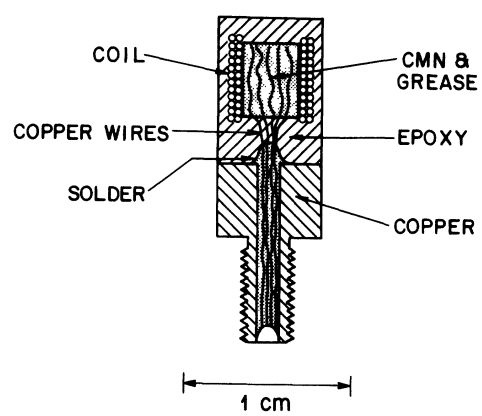

FIG. 5. CMN thermometer.

empty coil; χ_0 is a background susceptibility; η is the fraction of the coil volume occupied by CMN (≈ 0.5); Λ is the Curie constant; and Δ is a constant with a magnitude expected to be $\lesssim 0.3$ mK, which, in this work, was set equal to zero. Equations (2)–(4) imply that the temperature is related to the frequency through a relation of the form

$$1/T = A/f^2 + B\,. \tag{5}$$

The constants A and B used in converting resonant frequency to temperature for $T < 0.9$ K were determined by a least-squares fitting of the T-f data obtained for $0.9 < T < 2.0$. Deviations of the measured temperatures from the calculated values are shown in Fig. 6.

E. Energy measurement

The energy input to the calorimeter due to the current pulse passing through the heater is given by $E = I^2Rt$, where I is the constant current, R is the resistance of the main heater, and t is the time for which the current flows through the heater. The magnitude of the current which was provided by an electronic constant current source was accurately determined by measuring (using a potentiometer) the voltage drop across a standard resistor in series with the heater. A relay with mercury-wetted contacts was used to switch the current from a dummy load resistor to the heater. A second pair of contacts in the relay which opened and closed within 0.2 msec of the first pair was used to trigger an electronic timer in order to accurately determine the duration of the current pulse. The magnitude of the constant current was selected so that the pulse lengths could be kept between $\frac{1}{2}$ and 2 min. The resistance of the Pt-W heater, measured using a four-wire technique, was found to increase by only 0.06% as the temperature was changed from 4 K to 50 mK. In calculating the energy inputs to the calorimeter, the resistance of the heater was assumed to be constant and equal to its value at 1 K, namely, 9359 Ω. Because the leads on the heater were superconducting there was no correction for heat generated in the leads. The total error in the energy measurement, is expected to be less than 0.04%.

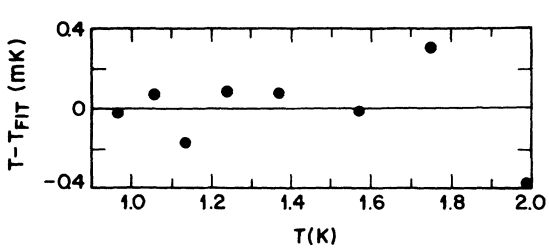

FIG. 6. Deviations of the CMN thermometer calibration data from the temperature determined using Eq. (5).

F. Procedure

All of the specific-heat data presented in this paper were obtained after a single cool down of the apparatus. During this run the thermometer bridges were also calibrated, and the heat capacity of the empty calorimeter was determined.

Several days were required to cool the apparatus from room to liquid-helium temperature since no hydrogen or helium exchange gas was used. Once liquid helium had been transferred into the main bath of the Dewar, which had been precooled to 77 K, the 1-K platform and the still of the dilution refrigerator (see Fig. 2) were slowly cooled to 4.2 K by liquid-helium reflux in the ^{4}He-refrigerator pump-out tube and in the shortening tube, respectively. During this process, which required about 24 h, a ^{4}He pressure of roughly 7 psi was maintained in these plumbing lines. The mixing chamber of the refrigerator and the calorimeter were thermally connected to the 1-K platform via the two mechanical heat switches and were thus also cooled to 4.2 K. Next the shorting tube was evacuated; the vise-type heat switch was opened; and the 1-K and dilution refrigerators were started. By the following morning the calorimeter was at 50 mK. Several days were now spent calibrating the thermometers (see Sec. II D) and measuring the heat capacity of the empty calorimeter (see Sec. II H).

The high-purity ^{3}He sample was then condensed into the calorimeter. About 20 h were required to completely fill the cell with liquid. The sample pressure was now increased at a rate that did not cause the calorimeter to warm excessively. To prevent any solid from forming in the capillary during this process, the temperatures of the capillary thermal anchors on the mixing chamber and on the 1-K platform were raised above the freezing temperature of the sample. When the pressure corresponding to the desired molar volume was reached, the pressure generator (see Sec. II C) was separated from the system. The calorimeter then started to cool slowly. After the freezing temperature had been reached, which was indicated by a dramatic decrease in the cooling rate, the heaters on the capillary thermal anchors were gradually turned off. With the capillary plugged with solid helium the sample in the calorimeter was now confined to solidify at constant average density. For the lowest-density sample

TABLE I. Melting temperature T_m and molar volume V_M for each of the bcc ^{3}He samples. The molar volumes were determined from T_m using the melting curve PVT data of Grilly (Ref. 34).

Sample	T_m (K)	V_M (cm^3)	Time required to solidify sample (h)
1	0.6743	24.454	42
2	0.9349	23.786	31
3	1.1820	23.081	20
4	1.4235	22.425	19
5	1.8114	21.459	13

this required 42 h (see Table I). The completion of solidification was marked by a sudden increase in the cooling rate. At this time the melting temperature T_m was accurately determined by slowly warming the sample and noting the onset of melting (see Fig. 7). The sharp change of slope in the warming curve indicates that the sample had a very uniform density. No further attempts to anneal the samples were made. The calorimeter was now allowed to cool overnight to approximately 47 mK. After opening the hydraulic heat switch and thereby allowing the calorimeter to slowly drift to its new equilibrium temperature (≈55 mK), heat-capacity measurements were begun.

The data were obtained using the conventional heat-pulse technique. Prior to each measurement, the power being dissipated in the auxiliary heater was increased by a small amount causing the calorimeter to warm at a slow and nearly constant rate. After this drift rate had been well established, a known amount of energy was delivered to the calorimeter which changed its temperature by approximately 5%. After thermal equilibrium had been reestablished the drift rate was again determined. The fore-drift rate for each datum point had been adjusted so that the after-drift rate, with the sample in thermal equilibrium, would be near zero. Extrapolations of the fore- and after-drifts to the middle of the heating interval were used to determined the temperature change ΔT due to the heat pulse. Data were taken in this manner to within a few mK of the melting temperature. If no more data were to be obtained at this density, T_m was again measured. The two determinations of T_m for each of the five densities agreed within the precision of the measurements (0.2 mK) and indicated that there was no slippage of the plug in the capillary.

For $T \gtrsim 0.2$ K and at each density only a few seconds were required for thermal equilibrium to be established. However at lower temperatures the thermal-relaxation times (spin-lattice relaxation) increased rapidly with increasing density (see Fig. 8) and at the two highest densities were so long that measurements could not be made for $T \lesssim 0.1$ K. At the middle density and for $T \lesssim 0.1$ K it was still necessary to monitor the temperature for at least 40 min after the heat pulse in order to determine the steady-state after-drift rate. As a result these low-temperature data are much less precise than those obtained for the two lowest densities where the thermal-relaxation times were much shorter.

G. Data reduction

The experimental information from which each heat-capacity datum point was derived consisted of an initial temperature T_i, a final temperature T_f, and the quantity of heat ΔQ responsible for the change in temperature. These three quantities are related to the heat capacity C_V via the relation

$$\Delta Q = \int_{T_i}^{T_f} C_V(T)\,dT\,. \tag{6}$$

If C_V is proportional to T^3, then this expression implies that

$$C_V(\overline{T}) = (\Delta Q/\Delta T)g\,, \tag{7}$$

where

$$g = 2\overline{T}^2/(T_i^2 + T^2{}_f) = \tfrac{1}{2}(1+\delta)^2/(1+\delta^2)\,,$$

$$\overline{T} = \tfrac{1}{2}(T_i + T_f)\,,$$

and

$$\delta = T_f/T_i\,.$$

In this work all of the data were obtained with $\delta \approx 1.05$. Thus in the region where C_V is roughly

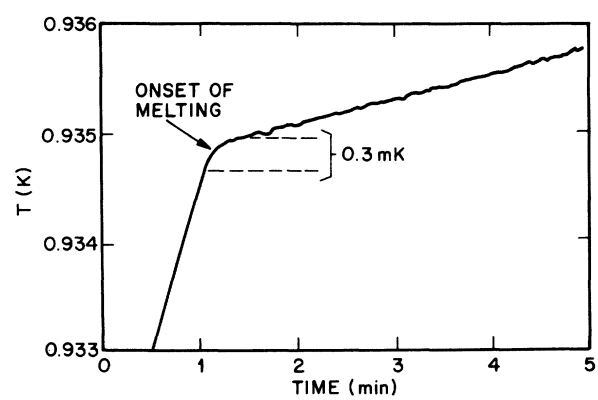

FIG. 7. Temperature as the calorimeter was warmed to the melting point of the sample vs time (arbitrary origin). The uncertainty in the melting temperature corresponds to an uncertainty in the molar volume of less than 10^{-3} cm^3.

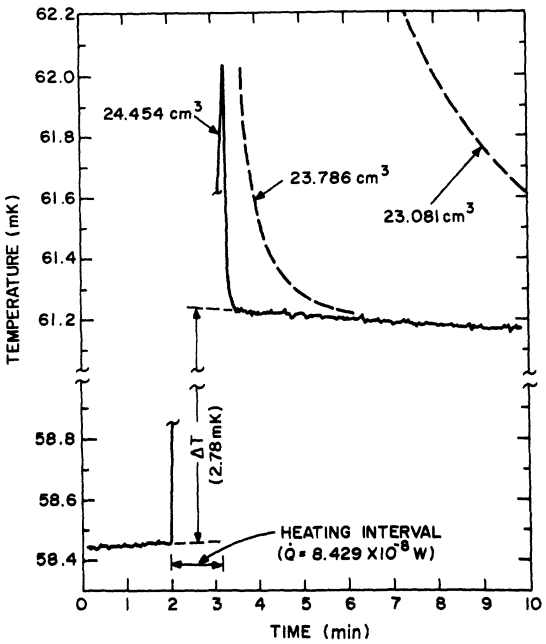

FIG. 8. Temperature recorded before and after the application of a heat pulse. The time axis has an arbitrary origin. The molar volume of the sample was 24.454 cm^3. At the higher densities, the longer thermal-relaxation times encountered at these low temperatures are indicated by the dashed curves.

proportional to T^3, i.e., for $T \gtrsim 0.1$ K, $g \approx 0.9994$. For $T \lesssim 0.1$ K, the heat capacity is roughly proportional to T^{-2}. Here g is given by the expression $4\delta/(1+\delta)^2$ which is again equal to 0.9994 for our particular value of δ. Thus calculating the heat capacity using Eq. (7) with g set equal to unity introduced an error of less than 0.1%.

The heat capacity of the sample is the measured heat capacity minus the heat capacity of the empty calorimeter. To convert this to a molar heat capacity the number of moles of sample was calculated using the measured sample-chamber volume and the molar volume of the sample. The molar volumes were determined using the measured melting temperature and the PVT data of Grilly.[34]

H. Heat capacity of the empty calorimeter

The contribution of the empty calorimeter to the total measured specific heat is shown in Fig. 9. For the largest sample molar volume (24.454 cm^3) at which measurements were made the empty cell was, at all temperatures, responsible for less than 35% of the total heat capacity. However, at the smallest molar volume considered (21.459 cm^3) the contribution of the empty cell became very significant at low temperatures and accounted for 80% of the total at 0.1 K. Obviously, this means that if, for example, the heat capacity of the empty and filled calorimeters were each measured with a precision of 1%, then the sample heat capacity at 0.1 K would be known only to 10%. It thus became extremely important for the higher density samples to know accurately the heat capacity of the empty as well as of the filled calorimeter.

The heat capacity of the evacuated calorimeter, measured at the beginning of the experiment, is plotted as C/T vs T^2 in Fig. 10. Figure 10(a) shows the data for $T < 2$ K, while Fig. 10(b) presents, in more detail, the data obtained for $T \lesssim 0.4$ K. A function of the form $AT + BT^3$ (straight lines in the figure) was adequate to describe the data above 0.4 K to within about 1%. However in order to fit the lower-temperature results it was necessary in addition to include a small constant term.

The dashed curve in Fig. 10 corresponds to the heat capacity one would have expected to measure if the calorimeter had been constructed entirely of copper. There were, of course, also small contributions to the specific heat from the stainless-steel filling capillary, the graphite support rods, the Pt-W heater wire, etc. The contribution from the ^{3}He exchange gas in the three germanium thermometers was mainly responsible for the need to add the constant term to the function in order to describe the low-temperature data. The thermometer capsules were filled by the manufacturer with a half-atmosphere of ^{3}He at room temperature. This implies that liquid should

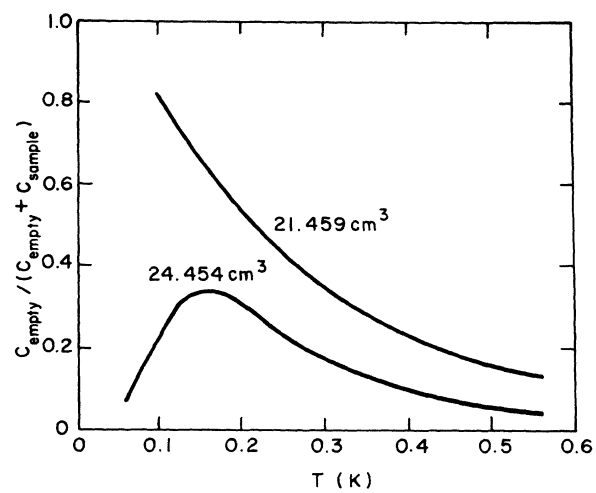

FIG. 9. Contribution of the empty calorimeter to the total measured heat capacity. The numbers give the molar volume of the sample.

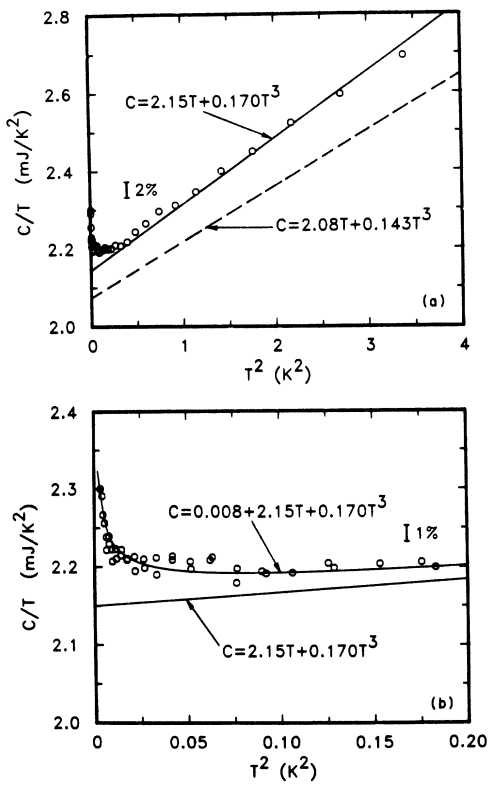

FIG. 10. Measured heat capacity of the empty calorimeter. The dashed line is the heat capacity of the equivalent mass of pure copper.

start to condense in these thermometers at roughly 0.8 K. Near this temperature ($T^2 \approx 0.6$ K^2) the data plotted in Fig. 10(a) do show a small anomalous peak. For $T \lesssim 0.5$ K the vapor pressure of ^{3}He is very small and so nearly all of the ^{3}He is in the liquid phase. The three thermometers, estimated to contain 5×10^{-6} moles of ^{3}He, will then contribute a roughly constant heat capacity of approximately 0.010 mJ/K for $0.15 \lesssim T \lesssim 0.5$ K ($0.023 \lesssim T^2 \lesssim 0.25$ K^2). At lower temperatures the specific heat of liquid ^{3}He decreases linearly with temperature. However, this decrease was apparently nearly offset by the growing $1/T^2$ contribution of the Pt-W heater wire. The specific heat of the CMN in the susceptibility thermometer also has a T^{-2} temperature dependence, however, its contribution was calculated to be only 0.2 μJ/K at 50 mK.

Because the filling capillary may have played a significant role in earlier specific-heat measurements on both solid ^{3}He and ^{4}He, we note here that the very small capillary used in this work accounted for less than 0.2% of the empty calorimeter's heat capacity at all temperatures.

III. RESULTS AND DISCUSSION

A. Absence of the low-temperature anomaly

The specific heat of bcc ^{3}He was measured at the five molar volumes listed in Table I. At the three largest volumes the data extend from 50 mK up to the melting curve; at the remaining two volumes data were obtained only above 0.1 K. Shown in Fig. 11 are the results for $T \lesssim 0.6$ K plotted as a function of temperature on log-log scales. For $T \lesssim 0.1$ K the specific heat is due mainly to the nuclear-spin contribution proportional to T^{-2} while at higher temperatures the phonon contribution proportional to T^3 dominates. Below roughly 0.1 K the scatter in the data increases rapidly with increasing density corresponding to the rapidly increasing thermal relaxation times encountered at low temperature (see Sec. II F). At the two highest densities these spin-lattice relaxation times were so long (>7 min) that meaningful data could not be obtained for $T \lesssim 0.1$ K.

The solid curve in Fig. 11 shows the smoothed results of Castles and Adams[4] at 24.40 cm^3/mole which is nearly equal to our largest molar volume. The two sets of measurements are in agreement at $T \approx 0.065$ K and for $T \gtrsim 0.3$ K; however, in the region of the minimum in the curves there is a large discrepancy of about 30%. Although not indicated in Fig. 11 a similar difference exists at the other molar volumes. Measurements of the

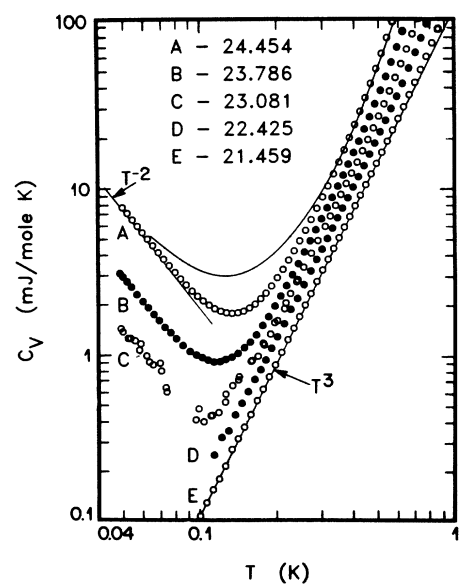

FIG. 11. Specific heat of bcc ^{3}He vs temperature. The numbers are the molar volumes in cm^3. The smooth curve corresponds to the work of Castles and Adams (Ref. 4) at 24.40 cm^3/mole.

specific heat by Sample and Swenson[2] and by Pandorf and Edwards[3] made prior to the work of Castles and Adams[4] do not extend in temperature to the region of the specific-heat minimum and so it is not possible to make as detailed a comparison with these results. However, in the region of temperature overlap these three earlier sets of data are qualitatively very similar. In the remainder of this section comparisons with previous measurements will mainly be restricted to the most recent work of Ref. 4.

Castles and Adams were able to describe their results, at each of the several molar volumes considered, by the function

$$C_V = \alpha T^{-2} + \beta T + \gamma T^3, \tag{8}$$

with β equal to 9, 8, and 7 mJ/mole K^2 at molar volumes of 24.40, 23.81, and 22.91 cm^3, respectively. A weighted[35] fit of the present data at the three largest volumes and for $T < 0.3$ K with the same function yielded values of 0.02 ± 0.05, 0.14 ± 0.05, and -0.9 ± 0.3 mJ/mole K^2 for nearly corresponding molar volumes of 24.454, 23.786, and 23.081 cm^3, respectively. The two sets of parameters differ by an order of magnitude in absolute value. Although the standard error bars on the present values of β do not include zero for each of the molar volumes, the deviation from zero is not considered to be significant. Small systematic errors in the measurements or the fact that other terms due to the lattice and proportional to higher powers of T should have been included in the fitting function could account for this difference. The present low-temperature results thus show no evidence for any contribution to the specific heat other than that attributable to the nuclear spins or to the phonons. The fact that the large anomalous contribution to the specific heat, reported in all of the previous specific-heat work on bcc ^{3}He, was not also observed in this work demonstrates that after all the long-standing specific-heat anomaly in ^{3}He is not due to some intrinsic property of this quantum solid. The origin of the anomaly in the previous work remains however an interesting matter.

At one time a similar anomaly had been reported in the specific-heat measurements[36-38] on hcp ^{4}He. But now it is generally believed that this excess contribution was due to various experimental difficulties such as an improper accounting of the large heat capacity of the stainless-steel filling capillary, errors in the low-temperature thermometer calibration, or errors in the measurement of the heating interval (see Ref. 39). It is possible though that crystal defects may have played a role in these measurements.[38] The more-recent measurements of the specific heat of hcp ^{4}He,[40-42] excepting the work of Castles and Adams[4] show no low-temperature anomaly. Castles and Adams do see an unexplained contribution to the specific heat but state that it is nearly within their experimental uncertainty. The absence of an anomaly in ^{4}He is consistent with the recent results of Hanson *et al.*[43] They observed no anomalous contribution to the entropy of the solid determined using high-resolution measurements of the density of liquid ^{4}He along the melting curve.

In the case of the most-recent specific-heat results on bcc ^{3}He by Castles and Adams care was taken to guard against some of the now-obvious pitfalls and still the anomaly remained. Since the present experiment differed in several technical respects from that of Castles and Adams and also from the other previous work it is not possible to definitely say which one of these differences explains why the anomalous specific heat was not also observed in the present work.

Table II is a comparison of some of the perhaps-significant experimental parameters in the present and in previous work on bcc ^{3}He. The differences which stand out are in the size of the calorimeter, in the ratio of surface area to volume, and also in the time used to solidify the sample. That the samples were grown extremely slowly and in a large calorimeter with a very open geometry suggests that the solid samples were of higher crystal quality than in the previous experiments. This leads to the speculation that crystal defects may have been responsible for the anomaly reported in the earlier works. It should also be noted that although Eq. (8) can be used to describe the data of Ref. 4, this does not imply that the term βT is the anomalous contribution to the specific heat. It has been shown[44] that if γ is required to be consistent with sound velocity measurements (and consequently also with the present results), then the excess specific heat of Ref. 4 has a Schottky-like temperature dependence. This again suggests crystal defects.[45] To be kept in mind, however, is the possibility that the excess specific heat observed previously may not in each experiment have been due to the same effect. If this is the case, then an intercomparison of the various experimental parameters can be both confusing and misleading. Another point to be considered, is the fact that the PVT measurements of Henriksen *et al.*,[46] which can be simply related to the specific heat, are consistent with the existence of the anomaly. Since these strain-gauge pressure measurements involve completely different experimental techniques and since there is no equivalent to the empty cell heat capacity to be subtracted from these data, it would appear that the specific heat anomaly cannot be dismissed as

TABLE II. Comparison of some experimental details.

	This work	Castles and Adams (Ref. 4)	Pandorf and Edwards (Ref. 3)	Sample and Swenson (Ref. 2)
Principal cell construction materials	Copper	BeCu and copper	Copper	BeCu
Nominal cell volume (cm^3)	9	1	0.3	1
Surface area/volume (cm^{-1})	6	275	10^4	10
$C_{empty}/(C_{empty}+C_{sample})$ at 0.3 K and at 24 cm^3/mole	0.2	0.4	0.6	0.4
Size of stainless-steel capillary	0.05-mm i.d. 0.15-mm o.d. by 8 cm long	0.10-mm i.d. 0.20-mm o.d. by 10 cm long	0.13-mm i.d. 0.25-mm o.d. filled with 0.08-mm-diam niobium wire	0.25-mm i.d. 0.46-mm o.d. filled with 0.2-mm-diam steel wire
$C_{capillary}/C_{empty}$ at 0.1 K	0.002	0.009	...	...
Transfer gas used in cool down	none	^{4}He	^{3}He	H_2
Heat switches	mechanical	superconducting (tin)	superconducting (indium)	mechanical and superconducting (lead)
^{4}He concentration (ppm)	2.4	2	300	1800
Freezing method	blocked capillary	blocked capillary	blocked capillary	blocked capillary
Solidification time (h)	13–42	1–2	<0.5	0.3
Annealing of sample after completion of solidification	no	yes (2 h)	yes	yes (0.3 h)
$\Delta T/T$	0.05	0.1–0.5	0.05	0.05
Temperature drift rate at 65 mk (μK/min)	10	400	...	...

having been due to some trivial experimental difficulty.

Table III gives the best-fit parameters when the data at the three lowest densities are fitted with Eq. (8) with β set equal to zero. In place of the α and γ values, the exchange energy $|J|/k_B$ and Debye temperature at 0 K, Θ_0, are listed. These parameters were calculated from α and γ using the relations

$$|J|/k_B = (\alpha/3R)^{1/2} \tag{9}$$

and

$$\Theta_0 = 12R\pi^4/5\gamma\,, \tag{10}$$

where k_B is Boltzmann's constant and R is the gas constant. The uncertainties quoted for each of the

TABLE III. Nuclear-exchange energies and Debye temperatures resulting from fits of the specific-heat data at the three largest molar volumes and below 0.3 K to the function $C_V = \alpha T^{-2} + \gamma T^3$.

Molar volume (cm^3)	$\|J\|/k_B$ (mK)	Θ_0 (K)
24.454	0.8756 ± 0.0006	18.91 ± 0.02
23.786	0.5435 ± 0.0008	20.52 ± 0.03
23.081	0.359 ± 0.007	21.97 ± 0.09

values in Table III are standard errors in the parameters. The additional systematic errors are difficult to estimate, but it is felt they are less than 0.5% for all of the parameters except for the value of $|J|$ at 23.081 cm^3/mole. At this density the long thermal-relaxation times at low temperatures may be responsible for a considerably larger systematic error. The deviations of the data at the two lowest densities from the best fit to Eq. (8) ($\beta \equiv 0$) are shown in Fig. 12. At the third molar volume the deviations are considerably larger and can readily be inferred directly from Fig. 11. In Fig. 13 the values of the exchange energy given in Table III are compared with those determined by others from specific heat,[4] magnetic susceptibility,[49] *PVT*,[48] and NMR[49] measurements. The molar volumes in all of the previous experiments have been redetermined using Grilly's[34] *PVT* data along the melting curve. The Debye temperature for the largest molar volume is in excellent agreement with the value determined from sound-velocity measurements[50] in single crystals of ^{3}He at 24.45 cm^3/mole, namely, 18.66 ± 0.34 K. The values of Θ_0 are also in agreement with the values determined from the previous specific-heat measurements by others[1-4] if their data below approximately 0.5 K are disregarded.

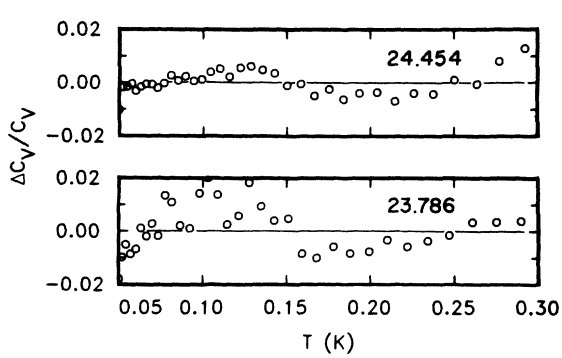

FIG. 12. Deviations from a least-squares fit of the specific-heat data to Eq. (8) with $\beta \equiv 0$. The numbers in the figure give the molar volumes in cm^3.

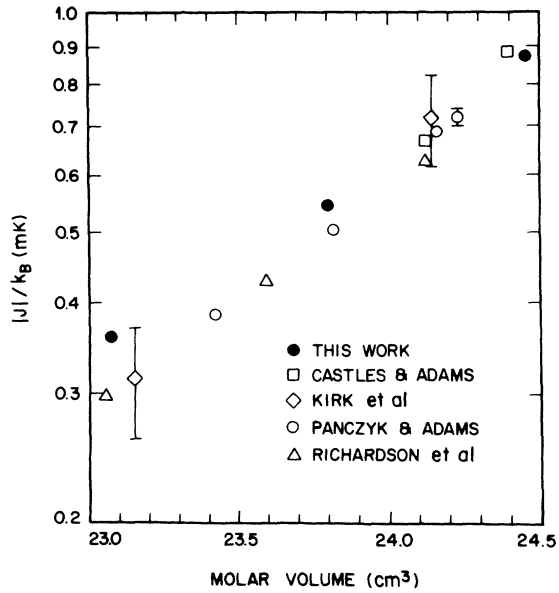

FIG. 13. Comparison of the nuclear-exchange energies determined in this work with values determined from specific-heat measurements by Castles and Adams (Ref. 4), from magnetic susceptibility measurements by Kirk *et al.* (Ref. 47), from *PVT* measurements by Panczyk and Adams (Ref. 48), and from NMR measurements by Richardson *et al.* (Ref. 49).

Further comparison of Θ_0 values is made in Sec. III B.

Another representation of the present specific heat results is given in Fig. 14. Plotted here is the temperature-dependent Debye theta $\Theta(T)$ calculated from the data at each of the five densities using the equation

$$C_V - C_V^{\text{spin}} = \tfrac{12}{5}\pi^4 R[T/\Theta(T)]^3 , \tag{11}$$

where

$$C_V^{\text{spin}} = \alpha T^{-2} = 3R(J/k_B T)^2 . \tag{12}$$

At the two highest densities the values of $|J|$ used were taken from the work of Panczyk and Adams.[48] If what remains after subtracting the spin-ordering contribution from the total measured specific heat of the sample is due to the lattice alone, then $\Theta(T)$ should be nearly constant for sufficiently low temperatures ($T/\Theta_0 \lesssim 0.02$). This is the behavior observed in most crystalline solids including hcp ^{4}He.[42] The present data at each of the densities are consistent with this expectation, but contrary to the rapid decrease in $\Theta(T)$ with decreasing temperature that has been reported on the basis of all of the previous C_V measurements[1-4] on bcc ^{3}He. The smoothed results of Castles and Adams are also indicated.

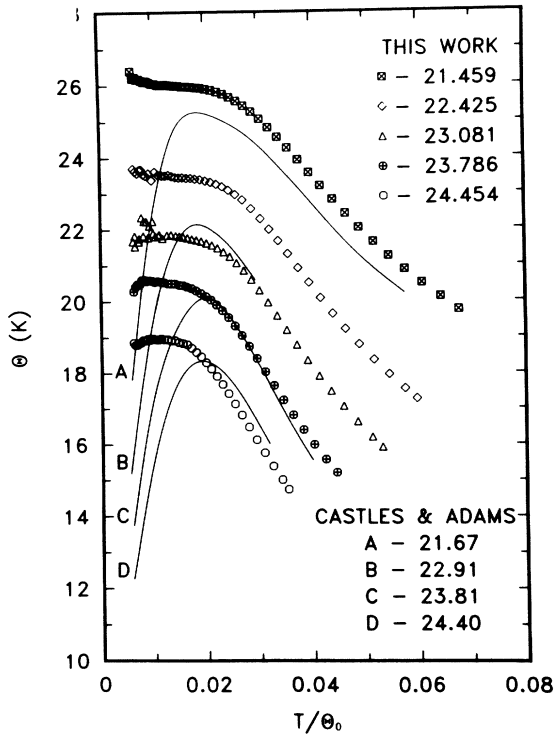

FIG. 14. Debye thetas for bcc ^{3}He vs reduced temperature. The numbers are the molar volumes in cm^3. The smooth curves were determined using the data of Castles and Adams tabulated in Ref. 4 with Θ_0 set equal to the maximum value of $\Theta(T)$.

The effects of errors in the determination of $|J|$ and in the heat capacity of the empty calorimeter upon $\Theta(T)$ are illustrated in Fig. 15. At the largest molar volume, 24.454 cm^3, a 1% error in $|J|$ has a very pronounced effect on Θ for $T/\Theta_0 \lesssim 0.01$. In contrast, at 21.459 cm^3/mole even a change in $|J|$ of 10% results in a significant change in Θ only for $T/\Theta_0 \lesssim 0.005$. Thus using values of $|J|$ determined in other experiments is not a serious problem at the higher densities. Also plotted in Fig. 15 are the changes in Θ corresponding to a 1% uncertainty in the heat capacity of the empty calorimeter. At the lowest density Θ is significantly modified only for $T/\Theta_0 \lesssim 0.005$, that is, for low enough temperatures that the exchange contribution is already appreciable. On the other hand, at the highest density the effects of an error in the addendum heat capacity of 1% would be seen in Θ at high enough temperatures so as to be distinguished from the effects of an error in $|J|$. Referring now to Fig. 14, the slight upward deviation of the data at 21.459 cm^3/mole and at the low-temperature end of the curve may be due to a systematic error in the heat capacity of the empty calorimeter of about 1%. The slight downward deviations of the data at the two largest molar volumes could be explained by an error in the determination of $|J|$ of less than a few tenths of 1%.

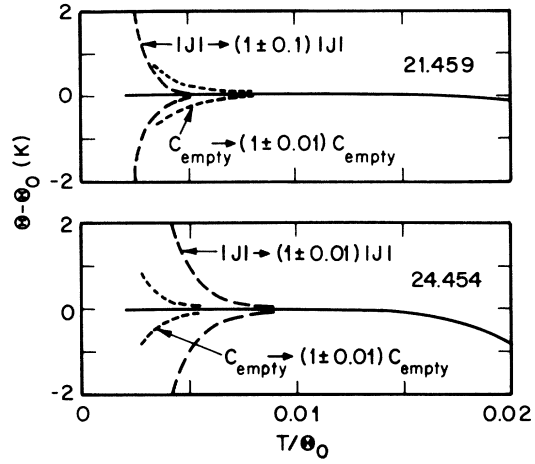

FIG. 15. Effects of errors in $|J|$ and in C_{empty} upon the determination of Θ. The numbers in the figure are the molar volumes in cm^3 of the highest- and lowest-density samples considered.

In this section of the paper the differences between the present and previous specific-heat measurements of bcc ^{3}He for $T \lesssim 0.5$ K have been discussed. At higher temperatures, however, all of the determinations of C_V are in reasonable agreement. This is demonstrated in Fig. 16, where Θ at 0.5 and at 1.0 K is plotted as a function of molar volume and compared with previous work.

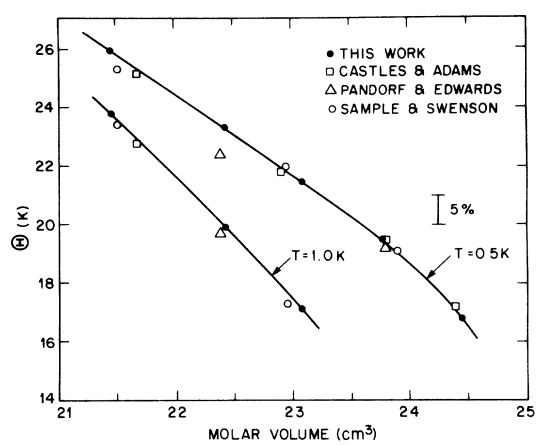

FIG. 16. Debye temperature as a function of molar volume along two isotherms. The results of Castles and Adams (Ref. 4), Pandorf and Edwards (Ref. 3), and Sample and Swenson (Ref. 2) are also shown for comparison.

TABLE IV. Values of the Debye temperature at 0 K, Θ_0, and the vacancy activation energy φ.

V_M (cm^3)	Θ_0	φ
24.454	18.95	5.99
23.786	20.53	6.99
23.081	21.90	8.05
22.425	23.54	9.24
21.459	26.04	11.22

B. Debye temperature and Grüneisen parameter

Listed in Table IV and plotted in Fig. 17 on log-log scales are values of the Debye temperature at 0 K determined for each of the molar volumes. The values, which at the three largest molar volumes differ slightly from those given in Table III, were determined by a graphical extrapolation of $\Theta(T)$ to 0 K (see Fig. 14). Also shown in Fig. 17 are values of Θ_0 determined by Sample and Swenson[2] and Castles and Adams[4] assuming Θ_0 to be equal to the maximum value of $\Theta(T)$. The negative of the slope of the straight line drawn through the present data, namely, 2.41, corresponds to the Grüneisen parameter at 0 K which is defined by the relation

$$\gamma_0 = \frac{-d\ln\Theta_0}{d\ln V}. \tag{13}$$

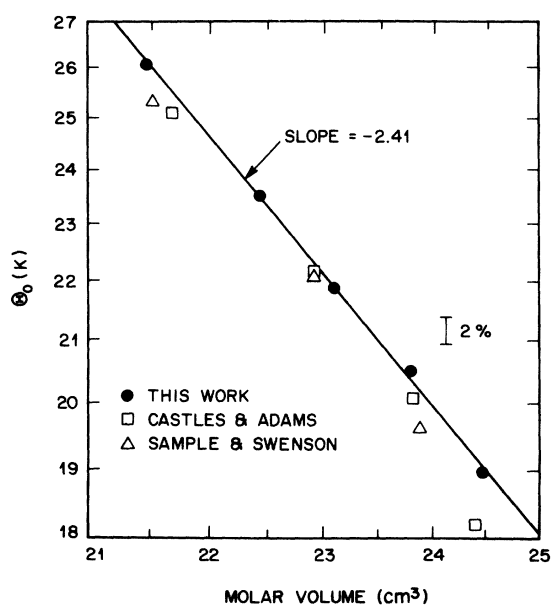

FIG. 17. Log-log plot of the Debye temperature at 0 K vs molar volume. Also shown are the results of Castles and Adams (Ref. 4) and Sample and Swenson (Ref. 2).

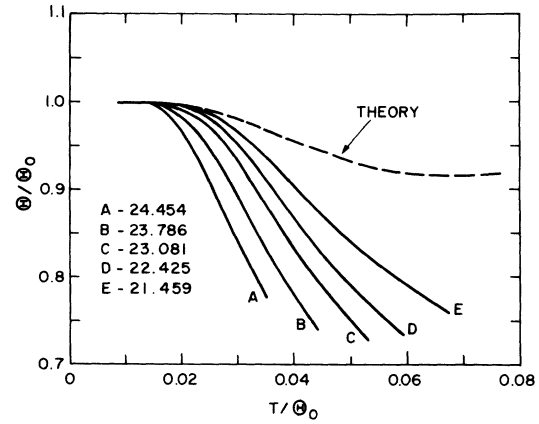

FIG. 18. Reduced plot of Debye theta vs temperature. The numbers are molar volumes in cm^3. The dashed curve corresponds to the vibrational specific heat calculated by de Wette *et al.* (Ref. 51).

The uncertainty in γ_0 is estimated to be ±0.05. Based on their estimates of Θ_0, Sample and Swenson had reported $\gamma_0 \approx 2.2$.

C. High-temperature anomaly

The smoothed specific-heat results are shown on a reduced plot of $\Theta(T)/\Theta_0$ vs T/Θ_0 in Fig. 18. In constructing this plot the values of Θ_0 listed in Table IV were used. In contrast to the nearly universal behavior observed for both hcp ^{3}He,[2] and ^{4}He,[41,42] at least for $T/\Theta_0 \lesssim 0.06$, the reduced curves in bcc ^{3}He have a large molar-volume dependence. This behavior is compared with the theoretical curve due to de Wette *et al.*[51] which is shown as a dashed line Fig. 18. The theoretical reduced curves determined using the calculated vibrational specific heat of bcc ^{3}He are density independent. We note also that the hcp ^{3}He,[2] and high-pressure hcp ^{4}He data,[41] as well as data for argon and krypton[52] (fcc) if plotted in Fig. 18 would agree to within about 1% with the dashed curve for $T/\Theta_0 \lesssim 0.06$. The fact that the experimental curves[1-3,53] for bcc ^{3}He deviate to such an extent from the expected behavior suggests that there is a significant contribution to the specific heat from some excitation system in addition to the phonons.

In Fig. 19(a) we show the excess specific heat as a function of temperature. The phonon contribution subtracted from the measured data was determined (after de Wette and Werthamer[54]) using values of the reduced Θ/Θ_0 from theory[51] and Θ_0 from experiment. This excess specific heat is the so-called "high"-temperature anomaly of bcc ^{3}He. In agreement with the observations of Heltemes and Swenson[1] and Sample and Swenson[2] the excess specific-heat results at each of the five densities

could be made to nearly coincide by scaling the temperature for each molar volume by a volume-dependent factor $f(V)$. Thus, in fitting the excess specific-heat data with an analytic function, it was only necessary to use the data at a single density. Since the data at the highest density cover the largest temperature range we tried fitting these results with the function

$$C_{\text{excess}} = R(g_1/g_0)(\varphi/T)^2 e^{-\varphi/T}. \tag{14}$$

This is the expression for the specific heat of a two-level system (Schottky specific heat) if $T \ll \varphi$. The ground state and excited state have degeneracies g_0 and g_1, respectively. The parameter φ is the energy separation between the two levels and $R = 8314$ mJ/mole K is the gas constant. The best fit value of φ with $g_1/g_0 = 1$ at this molar volume and values of φ at the other molar volumes determined using the relation

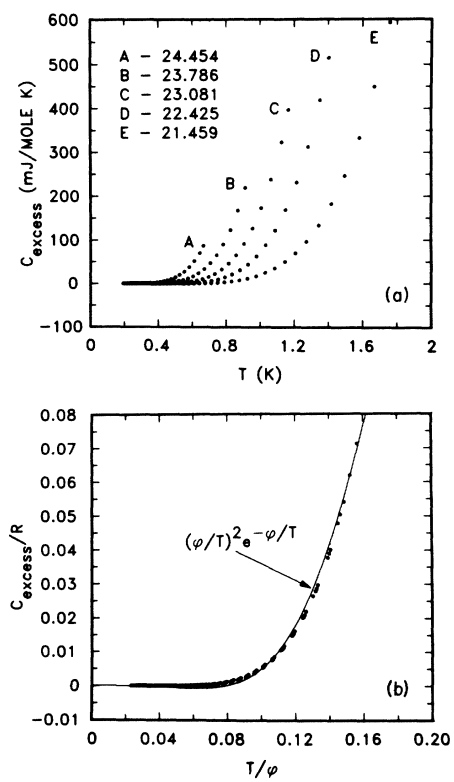

FIG. 19. (a) Excess specific heat vs temperatures. C_{excess} is the difference between the measured specific heat and the vibrational specific heat determined using the theoretical reduced Θ curve (Fig. 18) and Θ_0 from this work. (b) C_{excess} plotted as a function of reduced temperature T/φ. The values of φ used in constructing this figure are listed in Table IV and plotted as a function of molar volume in Fig. 20. The solid curve is the Schottky specific heat.

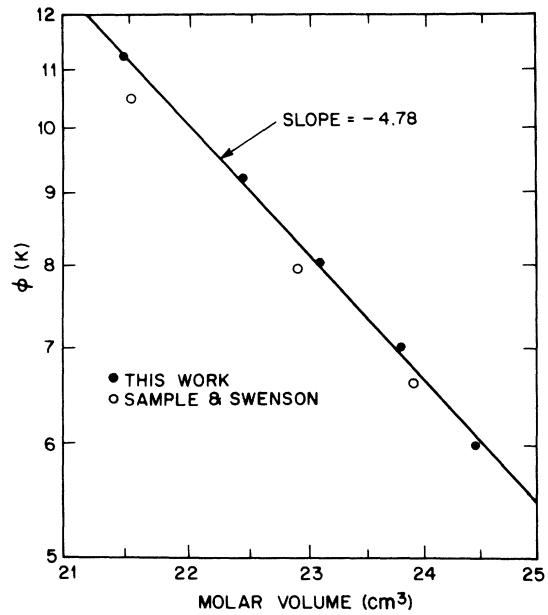

FIG. 20. Energies φ used to reduce the temperature in creating a universal curve for C_{excess} (see Fig. 19) plotted vs molar volume on log-log scales. The values of φ have been scaled so as to give the best fit to the Schottky function, Eq. (14).

$$\varphi(V) = f(V)\varphi(21.459)/f(21.459) \tag{15}$$

are plotted as a function of V on log-log scales in Fig. 20 and are listed in Table IV. The excess specific heat for each of the molar volumes divided by the gas constant is shown plotted versus the scaled temperature T/φ in Fig. 19(b). Also shown is the best-fit Schottky specific heat. Quite clearly there are significant systematic deviations of the data from the curve. These deviations are similar to those reported by de Wette and Werthamer[54] in their analysis of the Sample and Swenson[2] data. Other fits of the data to Eq. (14), with g_1/g_0 equal to 0.5, 3.5, 4.0 were definitely worse. The deviation of the data from the Schottky function are shown in greater detail in Fig. 21. They do not fall on a single curve, however, the deviations for each density are sensitive to the value of Θ_0 used in determining the excess specific heat and also depend on the point ($T/\varphi \approx 0.11$) at which the excess specific-heat curves were forced to coincide. For the largest molar volume (24.454 cm^3) and at $T \approx 0.4$ K ($T/\Theta_0 \approx 0.02$, $T/\varphi \approx 0.07$) the deviations correspond to the measured specific heat being approximately 10% larger than the sum of the phonon and Schottky contributions. It is not likely that this difference can be entirely attributed to the use of an incorrect phonon contribution since to correct the discrepancy it would be

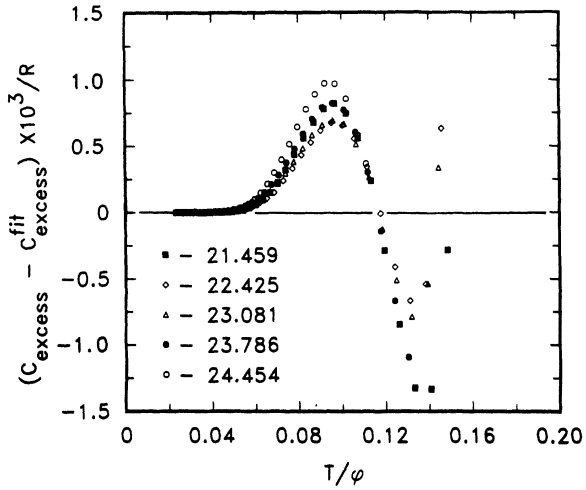

FIG. 21. Deviations of C_{excess} (see Fig. 19) from the Schottky function [Eq. (14), $g_1/g_0=1$] as a function of reduced temperature T/φ.

necessary to depress the phonon Θ/Θ_0 curve at $T/\Theta_0 \approx 0.02$ (see Fig. 18) by about 3%. This would place the phonon reduced-Debye-temperature curve at this reduced temperature below the measured (and hence also the phonon) Θ/Θ_0 curves at the highest densities. The Θ/Θ_0 curves corresponding to the vibrational specific heat would thus be required to have both a strong temperature and molar-volume dependence.

Results from specific heat,[1-3,53] thermal conductivity,[55,56] nuclear magnetic resonance,[57,58] and x-ray experiments[59,60] taken together give strong evidence that thermally activated vacancies are (at least partially) responsible for the anomalous specific heat. The significant deviations of the excess specific heat from the Schottky function however indicate that the excitation process is more complicated than simple vacancy formation. Hetherington[61] showed that a vacancy would be highly nonlocalized and would propagate as a wave in ^{3}He crystals. This calculation yields a band of vacancy excitation energies which lies considerably above the experimental values but has a similar molar volume dependence. In Guyer's[62] discussion of the properties of vacancy-wave excitations he gives an expression for the vacancy-wave specific heat which is just Eq. (14) modified by a factor $F(T)$. The factor $F(T)$ is monotonically increasing and approaches unity as $T\to\infty$ and is a measure of how much of the band is filled at temperature T. The modified Schottky function increases with increasing T more rapidly than the Schottky function and hence deviates even more from the data in the region around $T/\varphi \approx 0.08$. Thus it appears that the high-temperature anomaly is not fully explained. It could be conjectured that there may be yet another excitation system but in any case it would appear that this unexplained contribution to the specific heat is in some way related to the vacancies since T/φ (see Fig. 21) remains a good reduced temperature.

Because of the systematic differences between the experimental excess specific heat and the Schottky function, the values of φ resulting from fits of those data to Eq. (14) depend strongly on the temperature range of the fit and on the weighting of the data. This, however, does not affect the density dependence of φ. The values of φ shown plotted versus the molar volume in Fig. 20 lie along a straight line with slope $d\ln\varphi/d\ln V_m = -4.74$. This slope is numerically equal to roughly twice the Grüneisen parameter γ. We thus find empirically that $\varphi \propto \Theta_0^2$.

D. Other thermodynamic functions

In order to facilitate the derivation of other thermodynamic functions, the specific-heat data minus the spin contribution at each molar volume were fitted with the polynomial

$$C_V^L \equiv C_V - C_V^{spin} = \sum_{n=3}^{N} A_n T^n . \tag{16}$$

Only data with $T/\Theta_0 > 0.008$ were included in the fits. C_V^{spin} was determined using the values of $|J|/k_B$ given in Table III for the three largest molar volumes. At 22.425 and 21.459 cm^3, respective values of 0.19 and 0.08 mK, taken from the work of Panczyk and Adams,[48] were used. The best-fit parameters are listed in Table V. Deviations of the data from the polynomials are plotted in Fig. 22. Above approximately 0.35 K, Fig. 22 demonstrates that the precision of the data is better than 0.1%. The larger scatter at lower temperatures is due to the longer thermal relaxation times encountered here (see Sec. II F) and also to the fact that significant contributions from the empty calorimeter (see Sec. II H) and from the nuclear spins (see Sec. III A) were subtracted from the total measured heat capacity.

In Table VI the smoothed values of $C_V - C_V^{spin}$ and the corresponding values of Θ/Θ_0 are tabulated as a function of T/Θ_0. Also listed are other thermodynamic functions. The entropy which can be written as a sum of lattice and spin contributions is related to the specific heat via the relation

$$S = S^L + S^{spin} = \int_0^T C_V T^{-1}\, dT , \tag{17}$$

where

$$S^L = \int_0^T C_V^L T^{-1}\, dT \tag{18}$$

TABLE V. Least-squares parameters determined by fitting the data (in units of mJ/mole K) at each molar volume with Eq. (16). Only data with $T > 0.008\ \Theta_0$ were included in the fits. Deviations from the polynomial approximations are plotted in Fig. 22.

Molar volume (cm^3)	$A_3\times10^{-2}$	$A_4\times10^{-2}$	$A_5\times10^{-2}$	$A_6\times10^{-3}$	$A_7\times10^{-4}$	$A_8\times10^{-4}$	$A_9\times10^{-3}$	$A_{10}\times10^{-2}$
24.454	2.009 150 1	14.845 158	−92.951 802	24.792 943	−2.620 186 1	1.046 510 2	...	...
23.786	2.310 416 7	−2.710 715 0	26.266 869	−11.153 310	2.305 078 2	−2.050 869 9	6.672 187 2	...
23.081	2.260 429 9	−9.151 338 8	66.479 731	−22.748 766	4.109 923 1	−3.924 622 7	19.032 906	−37.079 058
22.425	1.893 079 9	−5.978 006 2	34.598 184	−10.038 687	1.570 845 1	−1.303 558 4	5.487 258 6	−9.262 868 9
21.459	0.988 514 04	0.642 690 15	−0.204 303 49	−0.500 161 90	0.119 462 25	−0.103 534 75	0.401 701 24	−0.590 090 63

and

$$S^{\text{spin}} = \int_0^T C_V^{\text{spin}} T^{-1}\, dT$$
$$= R\ln 2 - \tfrac{3}{2}R(J/k_B T)^2 . \qquad (19)$$

For $T/\Theta_0 > 0.01$, $\frac{3}{2}R(J/k_B T)^2 < 10^{-4} R\ln 2$ for each of the molar volumes. Thus, to a very good approximation, the total entropy at these temperatures can be determined by simply adding $R\ln 2$ to S^L. In the table values of S^L are listed which were calculated using

$$S^L = \sum_{n=3}^{N} \frac{A_n}{n} T^n . \qquad (20)$$

The increase in the internal energy above its value at 0 K due to the lattice was determined using

$$(U - U_0)^L = \int_0^T C_V^L\, dT \qquad (21)$$

$$= \sum_{n=3}^{N} \left(\frac{A_n}{n+1}\right) T^{n+1} . \qquad (22)$$

The derivative $(\partial P/\partial T)_V$ can be related to the specific heat via the equations

$$\left(\frac{\partial P}{\partial T}\right)_V = \left(\frac{\partial P}{\partial T}\right)_V^L + \left(\frac{\partial P}{\partial T}\right)_V^{\text{spin}} = \left(\frac{\partial S}{\partial V}\right)_T , \qquad (23)$$

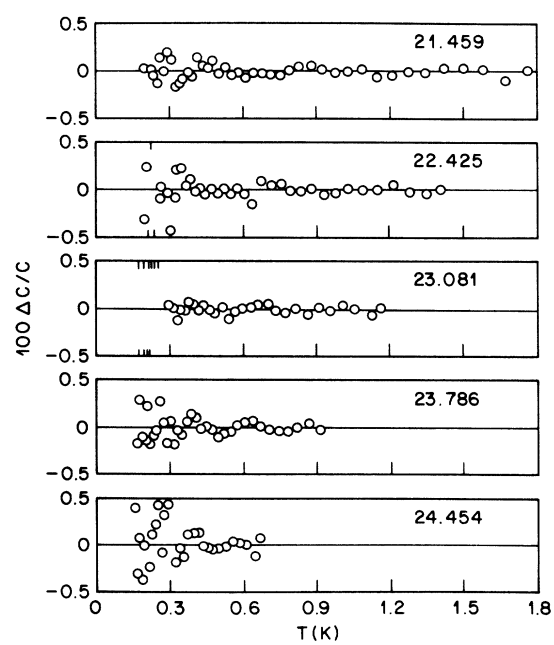

FIG. 22. Deviations from a least-squares fit of the specific-heat data with Eq. (16). The best-fit parameters are given in Table V. The numbers in the figure are the molar volume in cm^3. The short vertical-line segments indicate deviations larger than $\frac{1}{2}$%.

TABLE VI. Smoothed thermodynamic functions for bcc ^{3}He. The values in the bottom row for each of the molar volumes correspond to extrapolations of the functions to the melting curve.

T/Θ_0	$C_V - C_V^{spin}$ (mJ/mole K)	Θ/Θ_0	S^L (mJ/mole K)	$(U-U_0)^L$ (mJ/mole)	$(\partial P/\partial T)_V^L$ (10^{-3} bar/K)	$(P-P_0)^L$ (10^{-3} bar)
			$V = 24.454$ cm^3, $\Theta_0 = 18.95$ K			
0.010	1.95	1.00	0.64	0.092	1.93	0.091
0.015	6.65	0.995	2.18	0.467	6.77	0.470
0.020	17.38	0.964	5.36	1.538	18.3	1.58
0.025	40.84	0.906	11.44	4.158	48.2	4.51
0.030	88.31	0.841	22.61	10.03	118	12.0
0.035	175.9	0.780	42.16	22.15	255	29.0
0.0356	190	0.773	45.2	24.2	280	32.2
			$V = 23.786$ cm^3, $\Theta_0 = 20.53$ K			
0.010	1.93	1.00	0.64	0.099	1.99	0.101
0.015	6.63	0.996	2.18	0.506	6.87	0.522
0.020	16.50	0.980	5.28	1.635	17.5	1.71
0.025	36.10	0.944	10.82	4.220	41.5	4.57
0.030	74.34	0.890	20.41	9.678	95.0	11.2
0.035	144.5	0.832	36.63	20.57	198	25.8
0.040	262.0	0.780	62.98	40.96	381	54.7
0.045	446.2	0.735	103.7	76.63	687	108
0.0455	471	0.730	109	81.7	730	117
			$V = 23.081$ cm^3, $\Theta_0 = 21.90$ K			
0.010	1.92	1.00	0.63	0.104	2.04	0.112
0.015	6.64	0.996	2.18	0.537	7.01	0.574
0.020	16.13	0.988	5.24	1.730	17.4	1.85
0.025	33.56	0.967	10.52	4.355	38.4	4.79
0.030	65.57	0.928	19.18	9.607	82.3	11.2
0.035	122.6	0.879	33.17	19.62	166	24.4
0.040	217.4	0.830	55.24	37.84	310	49.9
0.045	364.0	0.787	88.72	69.12	546	96.0
0.050	579.3	0.749	137.5	120.0	909	175
0.0540	813	0.722	190	180	1260	263
			$V = 22.425$ cm^3, $\Theta_0 = 23.54$ K			
0.010	1.94	1.00	0.66	0.115	2.10	0.124
0.015	6.62	0.997	2.20	0.582	7.17	0.632
0.020	15.90	0.993	5.24	1.853	17.5	2.03
0.025	32.41	0.979	10.40	4.606	37.1	5.13
0.030	61.25	0.950	18.61	9.961	74.6	11.5
0.035	110.7	0.910	31.44	19.83	144	24.0
0.040	191.4	0.866	51.08	37.25	262	47.5
0.045	314.6	0.826	80.26	66.55	449	88.7
0.050	492.3	0.790	122.1	113.4	737	158
0.055	739.6	0.759	180.0	185.2	1150	268
0.060	1073	0.731	258.0	290.0	1670	433
0.0605	1110	0.729	266	303	1710	446
			$V = 21.459$ cm^3, $\Theta_0 = 26.04$ K			
0.010	1.94	1.00	0.64	0.125	2.19	0.142
0.015	6.60	0.998	2.18	0.641	7.44	0.725
0.020	15.79	0.995	5.21	2.039	18.0	2.31
0.025	31.78	0.985	10.29	5.044	36.8	5.77
0.030	58.47	0.965	18.24	10.78	69.5	12.5
0.035	101.7	0.936	30.25	20.99	127	25.0
0.040	169.2	0.903	47.92	38.32	221	47.1
0.045	269.1	0.870	73.26	66.45	365	84.7
0.050	410.0	0.840	108.5	110.2	578	145
0.055	600.7	0.813	156.1	175.4	886	240

TABLE VI. (*Continued*).

T/Θ_0	$C_V - C_V^{spin}$ (mJ/mole K)	Θ/Θ_0	S^L (mJ/mole K)	$(U-U_0)^L$ (mJ/mole)	$(\partial P/\partial T)_V^L$ (10^{-3} bar/K)	$(P-P_0)^L$ (10^{-3} bar)
			$V = 21.459$ cm^3, $\Theta_0 = 26.04$ K			
0.060	851.7	0.790	218.6	269.2	1300	381
0.065	1176	0.768	299.1	400.3	1830	584
0.0696	1550	0.751	391	561	2380	832

where

$$\left(\frac{\partial P}{\partial T}\right)_V^L = \left(\frac{\partial S^L}{\partial V}\right)_T = \int_0^T T^{-1}\left(\frac{\partial C_V^L}{\partial V}\right)_T dT \tag{24}$$

and

$$\left(\frac{\partial P}{\partial V}\right)_V^{spin} = \left(\frac{\partial S^{spin}}{\partial V}\right)_T = \frac{-3R}{V}\left(\frac{J}{k_B T}\right)^2 \frac{d\ln|J|}{d\ln V}. \tag{25}$$

In order to compute $(\partial P/\partial T)_V^L$ it was necessary to express C_V^L as a smooth function of the volume so that the volume derivative could be accurately determined. This was done by writing

$$C_V^L = C_{ph} + C_{Sch} + C_{dif}. \tag{26}$$

As in Sec. III C, the phonon contribution to the specific heat C_{ph} was taken as

$$C_{ph} = \tfrac{12}{5}R\pi^4(T/\Theta)^3, \tag{27}$$

with

$$\Theta = \Theta_0(\Theta/\Theta_0)_{theory} \tag{28}$$

and

$$\left(\frac{\Theta}{\Theta_0}\right)_{theory} = \sum_{n=1}^{8} C_n\left(\frac{T}{\Theta_0}\right)^{n-1}. \tag{29}$$

The theoretical curve for the reduced Debye temperature is due to de Wette *et al.*[15]; the coefficients C_n in the polynominal approximation are given in a paper by de Wette and Werthamer.[54] Values of Θ_0 were determined as a function of the molar volume using (see Sec. III B)

$$\Theta_0 = 4.188\times 10^4 V^{-2.407}. \tag{30}$$

The second term of Eq. (26) is the Schottky contribution to the specific heat (see Sec. III C) given by Eq. (14) with

$$\varphi = 2.584\times 10^7 V^{-4.775}. \tag{31}$$

The final term in Eq. (26), C_{dif}, accounts for the difference between C_V^L and the sum of the phonon and Schottky contributions. In Sec. III C, this difference was labeled $C_{excess} - C_{excess}^{fit}$ and plotted as a function of T/φ in Fig. 21. For the purposes of the present calculations these deviations were described by the function

$$C_{dif} = -0.075R(T/\varphi - 0.115) \times e^{-1250(T/\varphi - 0.115)^2}.$$

Smoothing of the results with respect to molar volume in this manner leads to calculated values of C_V^L which differed from the data by as much as 5% at the largest molar volume. This is apparent from the deviations of both Θ_0 and φ from the best-fit curves [Eqs. (30) and (31), respectively] drawn in Figs. 17 and 20. These deviations of Θ_0 and φ are largest for the two largest molar volumes and appear to be correlated: the same adjustment in the molar volumes is required to bring both the Θ_0 and φ values onto the respective solid curves. Using adjusted molar volumes (e.g., 24.454 → 24.53 cm^3/mole), the deviations of the specific-heat data from Eq. (26) were less than about 1% for each density. The values of $(\partial P/\partial T)_V^L$ listed in Table II were determined by numerically evaluating the integral of Eq. (24) using the adjusted molar volumes.

The final column in Table II gives the integral of this derivative with respect to temperature; that is, it lists the change in pressure above its value at absolute zero which is due to the lattice. For $T > 0.4$ K, the spin contribution to the pressure is small, and thus the tabulated values can be used in a comparison with the direct measurements of pressure versus temperature by Straty and Adams.[63] The two sets of data are in good agreement.

IV. SUMMARY

Using a large copper calorimeter with a very open geometry, the specific heat at constant volume of bcc ^{3}He was measured with high precision at five molar volumes. The high-purity ^{3}He sample was solidified extremely slowly using the blocked-capillary method. At the three largest molar volumes, the data extend from the melting curve down to 50 mK. Below approximately 100 mK these data are dominated by the T^{-2} contribution due to the nuclear spins and yield values of

the nuclear exchange energy in agreement with other measurements. At the two highest densities the data extend down in temperature to 100 mK. No data could be obtained at lower temperatures due to very long thermal-relaxation times. When the spin contribution is subtracted from the data at each of the five molar volumes, the results below approximately 0.3 K are proportional to T^3, the temperature dependence expected for the phonon contribution. In contrast to all of the previous specific-heat measurements on bcc ^{3}He, the present results show no evidence of any anomalous contribution. Thus the long-standing low-temperature specific-heat anomaly of ^{3}He, cannot be due to an intrinsic property of this quantum solid. The source of the anomaly seen by others is still however unknown.

At temperatures greater than about 0.5 K the present results are in agreement with the earlier less-precise measurements and show a significant contribution to the specific heat which presumably is due to some excitation system in addition to the phonons. This contribution has generally been attributed to the presence of thermally activated vacancies. As in the earlier works the temperature dependence of this excess specific heat can be qualitatively described by the Schottky function corresponding to the specific heat of a two-energy-level system. In the present work, however, the specific-heat data are not complicated by the presence of the low-temperature anomaly, and thus Θ_0 for each volume could be determined accurately. This permitted the vacancy contribution to be extracted from the data with less uncertainty than previously possible. These excess specific-heat data show significant systematic deviations from the simple Schottky function. At the largest molar volume this difference corresponds to as much as 10% of the sample's total heat capacity. The expression for the specific-heat due to vacancy waves given by Guyer deviates even more from the data.

The specific heat and other thermodynamic functions derivable from the specific heat have been tabulated for each of the five molar volumes.

---

[1]E. C. Heltemes and C. A. Swenson, Phys. Rev. 128, 1512 (1962).

[2]H. H. Sample and C. A. Swenson, Phys. Rev. 158, 188 (1967).

[3]R. C. Pandorf and D. O. Edwards, Phys. Rev. 169, 222 (1968).

[4]S. H. Castles and E. D. Adams, Phys. Rev. Lett. 30, 1125 (1973); and J. Low Temp. Phys. 19, 397 (1975).

[5]C. M. Varma, Phys. Rev. Lett. 24, 203, 970(E) (1970).

[6]H. Horner, J. Low Temp. Phys. 8, 511 (1972).

[7]R. A. Guyer, J. Low Temp. Phys. 6, 251 (1972).

[8]I. E. Dzyaloshinskii, P. S. Kondratenko, and V. S. Levchenkov, Zh. Eksp. Teor. Fiz. 62, 1574 (1972) [Sov. Phys.-JETP 35, 823 (1972)]

[9]D. S. Greywall, Phys. Rev. B 11, 4717 (1975).

[10]J. P. Frank and I. D. Calder, in *Proceedings of the Fourteenth International Conference on Low-Temperature Physics, Otaniemi, Finland, 1975,* edited by M. Krusius and M. Vuorio (North-Holland, Amsterdam, 1975), Vol. 1, p. 495.

[11]A. Widom and J. B. Sokoloff, J. Low Temp. Phys. 21, 463 (1975).

[12]J. B. Sokoloff and A. Widom, Phys. Rev. Lett. 35, 673 (1975).

[13]D. S. Greywall, Phys. Rev. Lett. 37, 105 (1976).

[14]Grade AGOT Nuclear Graphite, Union Carbide Corp., Carbon Products Div., New York, N. Y.

[15]A fourth (identical) graphite tube was tested for mechanical strength. The tube fractured (near the middle) under an axial load of 44 lb.

[16]Brazing alloy: 72% silver, 28% copper.

[17]Sigmund Cohn Corp., Mount Vernon, N. Y.

[18]W. F. Giauque, D. N. Lyon, E. W. Hornung, and T. E. Hopkins, J. Chem. Phys. 37, 1446 (1962).

[19]J. C. Ho and N. E. Phillips, Rev. Sci. Instrum. 36, 1382 (1965).

[20]O. V. Lounasmaa, *Experimental Principles and Methods Below 1 K* (Academic, London and New York, 1974), Chap. 9.

[21]R. H. Sherman, in *Proceedings of the Tenth International Conference on Low Temperature Physics* (VINITI, Moscow, 1967), Vol. 1, p. 188.

[22]United States Bureau of Mines, Helium Operations, Amarillo, Tex.

[23]Cryo Cal, Inc., Riviera Beach, Fla.

[24]Scientific Instruments, Inc., Lake Worth, Fla.

[25]G. Ahlers, Phys. Rev. 171, 275 (1968). See also K. H. Mueller, G. Ahlers, and F. Pobell, Phys. Rev. B 14, 2096 (1976).

[26]R. H. Sherman, S. G. Sydoriak, and T. R. Roberts, J. Res. Natl. Bur. Stand. (U.S.) A 68, 579 (1964).

[27]D. S. Betts, D. T. Edmonds, B. E. Keen, and P. W. Matthews, J. Sci. Instrum. 41, 515 (1964).

[28]C. Boghosian, H. Meyer, and J. E. Rives, Phys. Rev. 146, 110 (1966).

[29]J. F. Jarvis, D. Ramm, and H. Meyer, Phys. Rev. 170, 320 (1968).

[30]R. T. Harley, J. C. Gustafson, and C. T. Walker, Cryogenics 10, 510 (1970).

[31]K. Andres and E. Bucher, J. Low Temp. Phys. 9, 267 (1972).

[32]C. T. Van Degrift, Ph.D. thesis (University of California, Irvine, 1974) (unpublished).

[33]General Electric BD6.

[34]E. R. Grilly, J. Low Temp. Phys. 4, 615 (1971).

[35]A weighting factor of C_V^{-2} was used which causes

$$\sum\left(\frac{C_V^{\text{meas}}-C_V^{\text{fit}}}{C_V^{\text{meas}}}\right)^2$$

to be minimized.

[36]F. J. Webb, K. R. Wilkinson, and J. Wilks, Proc. R. Soc. Lond. A 214, 546 (1952).

[37]E. C. Heltemes and C. A. Swenson, Phys. Rev. 128,

1512 (1962).
[38]J. P. Franck, Phys. Lett. 11, 208 (1964).
[39]J. K. Hoffer, Ph.D. thesis (University of California, Berkeley, 1968) (unpublished), p. 21.
[40]D. O. Edwards and R. C. Pandorf, Phys. Rev. 140, A816 (1965).
[41]G. Ahlers, Phys. Rev. A 2, 1505 (1970); Phys. Lett. 22, 404 (1966).
[42]W. R. Gardner, J. K. Hoffer, and N. E. Phillips, Phys. Rev. A 7, 1029 (1973).
[43]H. N. Hanson, J. E. Berthold, G. M. Seidel, and H. J. Maris, Phys. Rev. B 14, 1911 (1976).
[44]D. S. Greywall, Phys. Rev. B 11, 4717 (1975).
[45]Y. Hiki, T. Maruyama, and Y. Kogure, J. Phys. Soc. Jpn. 34, 725 (1973).
[46]P. N. Henriksen, M. F. Panczyk, S. B. Trickey, and E. D. Adams, Phys. Rev. Lett. 23, 518 (1969).
[47]W. P. Kirk, E. B. Osgood, and M. Garber, Phys. Rev. Lett. 23, 833 (1969).
[48]M. F. Panczyk and E. D. Adams, Phys. Rev. 187, 321 (1969).
[49]R. C. Richardson, E. Hunt, and H. Meyer, Phys. Rev. 138, A1326 (1965). Corrected data are given in H. Meyer, J. Appl. Phys. 39, 390 (1968).
[50]D. S. Greywall, Phys. Rev. B 11, 1070 (1975).
[51]F. W. de Wette, L. H. Nosanow, and N. R. Werthamer, Phys. Rev. 162, 824 (1967).
[52]L. Finegold and N. E. Phillips, Phys. Rev. 177, 1383 (1969).
[53]D. O. Edwards, A. S. McWilliams, and J. G. Daunt, Phys. Lett. 1, 218 (1962).
[54]F. W. de Wette and N. R. Werthamer, Phys. Rev. 184, 209 (1969).
[55]B. Bertman, H. A. Fairbanks, C. W. White, and M. J. Crooks, Phys. Rev. 142, 74 (1966).
[56]W. C. Thomlinson, J. Low Temp. Phys. 9, 167 (1972).
[57]H. A. Reich, Phys. Rev. 129, 630 (1963).
[58]N. Sullivan, G. Deville, and A. Landesman, Phys. Rev. B 11, 1858 (1975).
[59]R. Balzer and R. O. Simmons, in *Proceedings of the Thirteenth International Conference on Low Temperature Physics, 1972,* edited by D. K. Timmerhaus, W. J. O'Sullivan, and E. F. Hammel (Plenum, New York, 1974), Vol. 2, p. 115.
[60]D. R. Baer and R. O. Simmons, Bull. Am. Phys. Soc. 21, 352 (1976).
[61]J. H. Hetherington, Phys. Rev. 176, 231 (1968).
[62]R. A. Guyer, J. Low Temp. Phys. 8, 427 (1972).
[63]G. C. Straty and E. D. Adams, Phys. Rev. 169, 232 (1968).

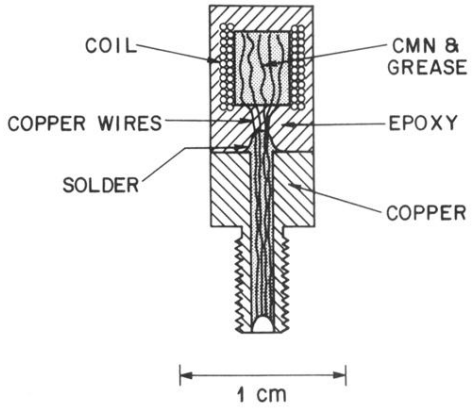

FIG. 5. CMN thermometer.